Pulsed ion beam-assisted carburizing of titanium in methane discharge*

M. Shafiq[a)], M. Hassan[b)†], K. Shahzad[a)], A. Qayyum[c)], S. Ahmad[c)], R. S. Rawat[d)], and M. Zakaullah[a)]

[a)] *Department of Physics, Quaid-i-Azam University,* 45320 *Islamabad, Pakistan*
[b)] *Department of Physics, GC University,* 54000 *Lahore, Pakistan*
[c)] *National Tokamak Fusion Program, P O Box* 3329 *Islamabad, Pakistan*
[d)] *Natural Sciences and Science Education, National Institute of Education, Nanyang Technological University, NIE BLK7, 1 Nanyang Walk, Singapore* 637616, *Singapore*

(Received 12 May 2009; revised manuscript received 13 June 2009)

The carburizing of titanium (Ti) is accomplished by utilizing energetic ion pulses of a 1.5 kJ Mather type dense plasma focus (DPF) device operated in methane discharge. X-ray diffraction (XRD) analysis confirms the deposition of polycrystalline titanium carbide (TiC). The samples carburized at lower axial and angular positions show an improved texture for a typical (200)TiC plane. The Williamson–Hall method is employed to estimate average crystallite size and microstrains in the carburized Ti surface. Crystallite size is found to vary from $\sim$ 50 to 100 nm, depending on the deposition parameters. Microstrains vary with the sample position and hence ion flux, and are converted from tensile to compressive by increasing the flux. The carburizing of Ti is confirmed by two major doublets extending from 300 to 390 cm^{-1} and from 560 to 620 cm^{-1} corresponding to acoustic and optical active modes in Raman spectra, respectively. Analyses by scanning electron microscopy/energy dispersive x-ray spectroscopy (SEM/EDS) have provided qualitative and quantitative profiles of the carburized surface. The Vickers microhardness of Ti is significantly improved after carburizing.

Keywords: carbide, plasma focus, microstructure, surface morphology
PACC: 2852, 5275P, 7690, 7470E

1. Introduction

The DPF device is a pulsed source of a short lived ($\sim$ 100 ns), dense ($10^{25} - 10^{26}$ m^{-3}) and high temperature (1–2 keV) plasma, which emits neutrons, x-rays, highly energetic ions and relativistic electrons.[1−4] The DPF device, being an efficient pulsed ion source, has been employed for materials processing including thin film deposition, phase change of thin films, ion implantation and surface modification over the last two and half decades.[5−12]

Titanium (Ti), a silvery ductile metal, finds tremendous applications in a variety of fields, in particular, aerospace and medical sciences, because of its excellent characteristics such as high strength-to-density ratio, remarkable corrosion resistance and biocompatibility. But the deprived tribological characteristics of Ti still limit its usages in adverse environmental and fatigue bearing conditions. In this regard, Ti is generally processed to change its surface properties. For instance, a thin hard protective coating of TiC on Ti and/or carbon ion implantation into it can remarkably improve its tribological characteristics. TiC is one of the most widely used industrial coating materials having significantly improved tribological properties such as high melting point, high strength and rigidity, excellent wear resistance and low friction coefficient, and is being used in abrasives, cutting tools, grinding wheels and cutting tips.[13] TiC is a potential material candidate for use as an electron injecting electrode in organic light emitting diodes (OLEDs) because of its good electrical conductivity and low work function.[14,15] It has been identified as a good container material for pyrochemical processing, owing to its good thermodynamic stability and thermal shock resistance.[16]

TiC coatings have been produced by using various methods such as chemical vapour deposition, arc ion plating, reactive sputtering and pulsed laser deposition, most of which require high deposition

*Project partially supported by the HEC research project at QAU Islamabad. One of the authors (K. Shahzad) is grateful to the NESCOM for providing financial support for his M. Phil studies.
†Corresponding author. E-mail: hassanjh@yahoo.com
© 2010 Chinese Physical Society and IOP Publishing Ltd

temperature.[17−20] The DPF device is a promising source in this respect, which offers room temperature deposition of thin films with better adhesion to the substrate, owing to broad energy spectrum of its ions. Moreover, it is an efficient pulsed power device which is simple, fast, cost-effective, little toxic and requires a short surface processing time (a few seconds for a few μm thick layer on substrate, with multiple shots used in deposition) as compared with other techniques. DPF ion-assisted depositions of well-adhered thin films of titanium carbide have recently been reported.[9,21] Gupta and Srivastava[9] used a 3.3 kJ Mather type DPF device equipped with a graphite carbon source to deposit TiC films on Ti substrate at room temperature by using multiple plasma focus shots. Rawat *et al.*[21] deposited TiC thin film on 304-stainless steel by using energetic carbon ions emitted from methane (CH_4) discharge of a DPF device, fitted with a solid titanium anode.

In the present investigations, we report on the carburizing of Ti by using energetic carbon ions emitted from a DPF device operated in CH_4 discharge, equipped with an engraved anode. The carburized Ti samples are characterized for their surface microstructure, surface morphology, chemical bond nature and elemental concentration in terms of deposition parameters (variations of axial and angular positions of samples).

2. Experimental setup

A schematic diagram of the DPF device used for the carburizing of Ti substrate is shown in Fig. 1.[1] It is a conventional Mather type plasma focus device operated at 1.5 kJ discharge energy, when powered by a 9 μF, 18 kV capacitor bank. The coaxial electrode assembly consists of a copper anode having an effective length of 100 mm and a diameter of 18 mm, surrounded symmetrically by six copper cathode rods each with a diameter of 9 mm in a squirrel cage fashion. A Pyrex glass insulator sleeve having an effective length of 25 mm supports a low inductance breakdown for the development of current sheath across the electrodes. The processing chamber of the device, which encloses the electrode assembly, is evacuated down to a pressure of 10^{-2} mbar (1 bar=10^5 Pa) by using a rotary van pump. CH_4 is used as the working gas at an optimum pressure of 2 mbar. A field distortion type pressurized spark gap acts as a fast switch to discharge the capacitor bank across the electrodes. The total parasitic inductance of the system is about 80 nH. A resistor divider is used as a high voltage probe to monitor the status of focusing, and a Rogowski coil records current waveform.

After closing the switch, a gas breakdown occurs in the gap between electrodes initially across the insulator sleeve, forming an umbrella-like current sheath. The azimuthal magnetic field located in toroidal volume enclosed by current produces a Lorentz force that pushes the sheath towards the open end of electrodes. The run-down of the current sheath is of a sweeping supersonic shock that propagates, ionizes and collects the gas particles ahead of the sheath front. On its arrival at the open end, the magnetic field starts to compress radially, accelerating the sheath toward the axis. Finally, the sheath converges onto the axis in the form of small and dense focused plasma. This is where the instant MHD-instabilities (mainly $m = 0$) start growing.[22] This in turn increases the electron temperature and induces intense electric fields. The rapid development of $m = 0$ (sausage) instability causes the necking of the focus plasma column, leading to its disruption. Immediately after disruption, ions and electrons are emitted. Ions are accelerated away from the anode and are used for the processing of the material specimen.

Commercially pure Ti substrates of 9 mm× 9 mm× 1 mm in dimension are polished by using a Metkon GRIPO 2V polishing machine with 600 to 2000 grit silicon carbide abrasive papers, followed by fine polishing with Brasso. The substrate samples are then ultrasonically cleaned with de-ionized water, acetone and ethanol sequentially for 15 min each. The samples are fixed onto a sample holder at 1 and 2 cm away from the anode axis and are respectively labelled as 'Off Centre' and 'Extreme'. The reason for treating Ti samples at these positions is to avoid surface damage that could be expected by treatment along the anode axis. The degradation of substrate surface quality at a smaller distance along the anode axis has been well reported in recent results of ion-assisted coatings by a low energy DPF device.[4] The sample holder is slightly curved to keep the distances of samples from the tip of anode identical and to ensure the ions incident normally on the substrate, which has a certain role in developing a particular crystallographic texture. Once good focusing of the plasma is achieved after a few conditioning shots, the shutter is removed. The samples are exposed for 20 focus shots each at distances of 8, 10 and 12 cm. After every 5 shots, the discharge chamber is evacuated and fresh gas is filled in order to minimize impurities in the discharge.

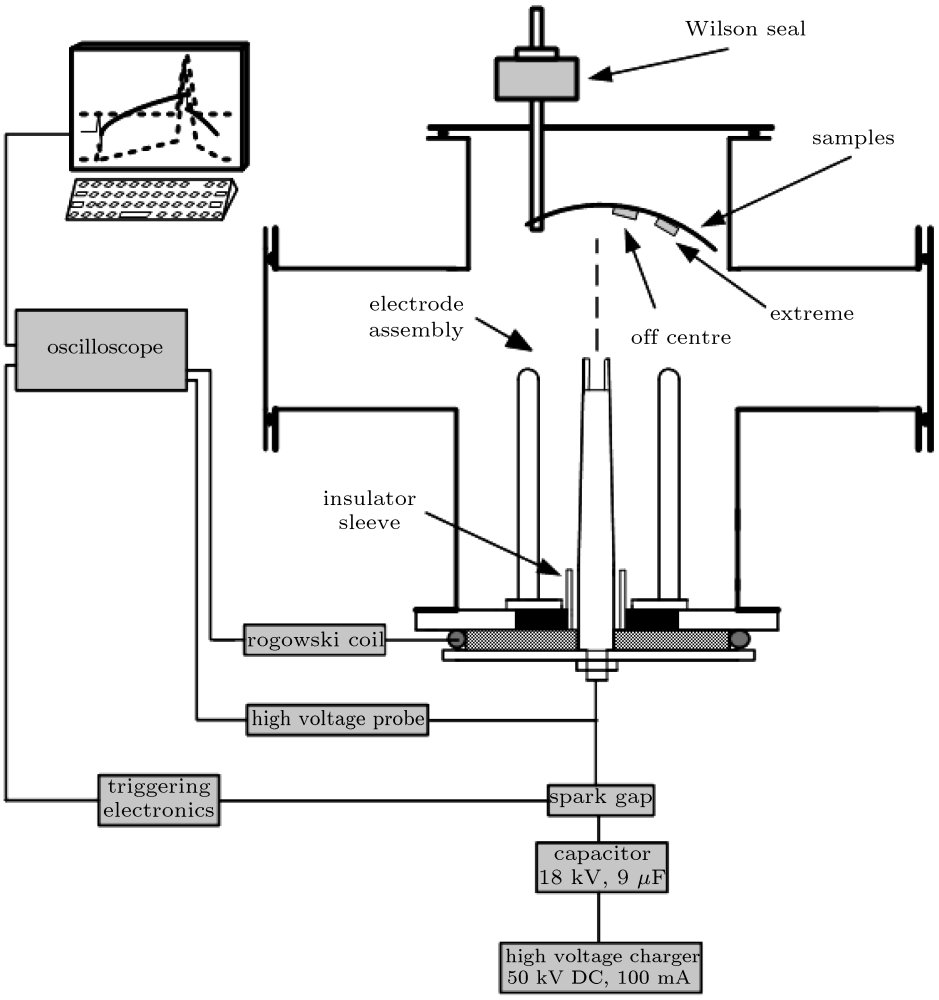


Fig. 1. Schematic diagram of the DPF device used for carburizing Ti.

The carburized Ti samples are analysed for their crystallography by employing X'Pert PRO XRD operated at 40 kV, using a Cu Kα (λ = 1.544 Å) radiation source. The surface morphology and elemental composition of the samples are revealed by employing a JEOL JSM-5910 SEM equipped with INCA 200; Oxford Instrum. UK, EDS attachment. SEM micrographs are recorded at a tube accelerating voltage of 5 kV, electron current of 10 μA and working distance varying from 3 to 8 mm. The EDS analysis is performed at a tube accelerating voltage of 10 kV with an electron current of 20 μA and a working distance of 15 mm. The spatial uniformity of carburized sample surfaces in terms of its elemental distribution is investigated by recording its elemental maps (Ti-Kα and C-Kα) using imaging energy filters. A Wilson Wolpert 401MVA Vickers microhardness tester is used for microhardness measurements of carburized Ti to test their mechanical strength.

3. Results and discussion

Figure 2 shows XRD patterns of Ti samples, ion irradiated at different axial (8, 10 and 12 cm) and angular positions (Off Centre and Extreme). The XRD spectra show diffraction peaks corresponding to (111), (200), (220) and (311) plane reflections of TiC at 2θ positions of 35.98°, 41.85°, 61.01° and 72.84° respectively. The respective peaks are confirmed by the pattern; 03-065-8805 of Powder Diffraction NIST data collection code: L14552, providing the standard peak positions respectively at 36.10°, 41.92°, 60.79° and 72.78°. The variation of relative peak intensity and the broadening of peaks of TiC by changing the sample position and hence varying ion energy and

flux show ion-induced re-crystallization, interstitial implantation of carbon as well as some defects in the substrate. The ion-induced collision cascades in the restructured substrate surface may also produce microstrains in it, which gives rise to slight shifts of diffraction peak positions from their corresponding standard data (addressed later in this section). Noticeably, the XRD spectra of substrate samples treated at all test positions show the variations of preferred texture based on axial and angular positions of samples. The evolution of a preferred plane orientation of TiC is still not fully understood.[23,24] The crystallographic texture evolution was explained on the basis of competition between strain energy and surface free energy.[25,26] Pelleg *et al.*[27] showed that TiC would grow in (200) preferred plane orientation at its initial stage because of its lowest surface energy. However, with deposition continuing, the coating grows, resulting in strain that competes with the surface energy to determine the orientation of the growing layer. Eventually, the strain energy associated with the layer becomes greater than the surface free energy resulting in a (111) orientation. This explanation for the preferred orientation is based solely on thermodynamic considerations without taking into account kinetic factors such as ion bombardment, composition, and incident ion angle and energy. Generally, for coatings deposited at low energy levels (i.e. low temperature, low ion bombardment), (111) crystallographic texture is observed.[28,29] The high deposition temperature favours significant surface diffusion and results in (200) crystallographic texture. It has been established that at lower substrate temperatures ($\leq 650^{\circ}$C), ion beam-assisted deposition can be used to control the degree of crystallographic texture, providing the amount and the energy of bombarding species are high enough.[28,29] The DPF is an efficient source of energetic ions and has been effectively employed for the deposition of various types of coatings on room temperature substrates. Therefore, the DPF ion-assisted deposition can be best tailored for the carburizing of metals. Analysis of integrated intensities for (111) and (200), (220) and (311) planes of TiC reveals crystallographic texture changes for different positions of the substrate during carburizing.

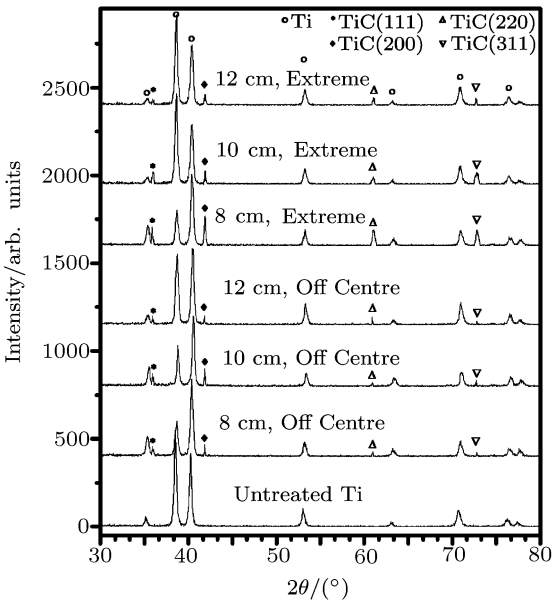


Fig. 2. X-ray diffraction patterns of Ti samples carburized at different axial and angular positions.

The texture coefficient for the favourably evolved plane orientation of TiC is evaluated from the expression[30,31]

$$\mathrm{TC}_{(hkl)} = \frac{I_{(hkl)}/I_{0(hkl)}}{N^{-1}\Sigma I_{(hkl)}/I_{0(hkl)}},$$

where $I_{(hkl)}$ is the estimated peak intensity, $I_{0(hkl)}$ is the standard intensity (from NIST data) and N is the number of plane reflections.

The texture coefficients calculated for a typical (200) preferred plane of TiC as a function of the axial distance for both angular positions are shown in Fig. 3. The maximum value of 1.19 is estimated for the sample carburized at the 10 cm axial and Off Centre angular position. This shows that TiC grows preferentially in the lowest surface energy (200) orientation as compared with the (111) orientation for this typical position of the sample during carburizing. At the 12 cm axial and Off Centre position, the texture coefficient of this (200) preferred plane decreases to 0.74. For the Extreme position of samples treated at three different axial distances (8, 10 and 12 cm), a maximum crystallographic texture coefficient of 0.86 is observed at 8 cm. Hence, microstructure evolves favourably at 10 cm and 8 cm axial positions with Off Centre and Extreme angular positions respectively. In fact, ion energy and ion flux each play a major role in the development of a particular texture. The DPF has been investigated to emit highly energetic ion beams with broad energy distribution, most of which are in the low energy tail. The above mentioned sample positions are found to be favourable for controlling ion energy and ion flux. A detailed discussion regarding the analyses of ion beam energy and ion flux and their role in the development of thin film coatings on Ti has been provided elsewhere.[4]

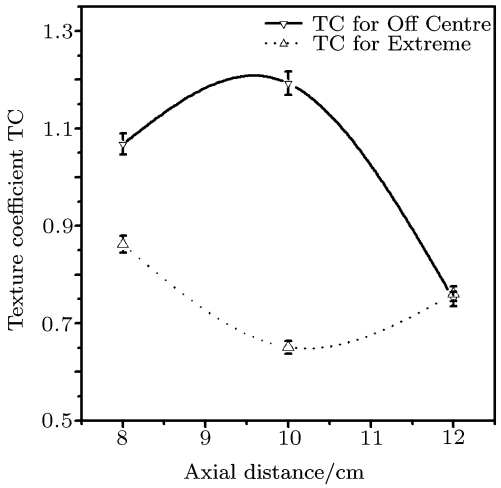


Fig. 3. Texture coefficient estimated from a typical (200) peak of TiC.

Thin coatings of materials deposited by various techniques usually contain residual internal stresses developed during condensation on the substrate. The DPF based thin coatings have residual strains/stresses owing to the energetic ion bombardment collision cascades and resulting significant fast cooling after transient temperature rise. Such strains/stresses have been evaluated by using x-ray diffraction data. The diffraction peak shifting from their corresponding stress-free data indicates uniform stresses/strains developed normal to the corresponding crystal plane in the film. XRD patterns show diffraction peak broadening owing to small crystallite size and large microstrains in the carburized Ti substrate surface. Microstrains in the restructured surface develop due to high density lattice defects mainly caused by atomic peening during energetic ion bombardment. For the evaluation of full width at half maximum (FWHM) for all plane reflections, the measured intensity patterns of diffraction peaks are fitted to a Gaussian function. The observed FWHM (B_0) is corrected for FWHM resulting from instrumental broadening (B_i) as measured from a standard polycrystalline silicon sample by using the following relation (for Gaussian broadening):[32]

$$B_\mathrm{r} = \sqrt{(B_0^2 - B_\mathrm{i}^2)}$$

where 'B_r' is the contribution of broadening due to crystalline imperfections, which can be separated into two contributions according to the Williamson–Hall (W–H) method in real space as follows:[33]

$$B_\mathrm{r} = k\lambda/L\cos\theta + \eta\tan\theta.$$

The first term on the right-hand side of the above expression is the contribution of broadening due to small crystallite size whereas the second term is the contribution of broadening due to lattice strain. A graphical plot of $B_\mathrm{r}\cos\theta$ versus $\sin\theta$ results in a straight line with slope η and intercept $k\lambda/L$. The crystallite size L can be determined from the intercept ($k = 0.94$) and microstrain can be determined from the slope.

Figure 4 shows W–H plots for Ti surfaces carburized at (a) Off Centre and (b) Extreme positions separately. From the W–H plots, the observed anisotropy in diffraction line broadening (some reflections are less broadened than most of the others) could be due to the anisotropic shape of the individual crystallite and/or the anisotropic dislocation strain field.[34] The average size and the average microstrain in a particular crystallographic direction from a set of (1st, 2nd, 3rd and 4th order) reflections in XRD patterns are determined by fitting a straight line to all data points corresponding to the observed reflections. The W–H plot for the sample carburized at the axial position of 8 cm, and Off Centre and Extreme angular positions are shown respectively in Figs. 4(a) and 4(b). Figure 4(a) shows

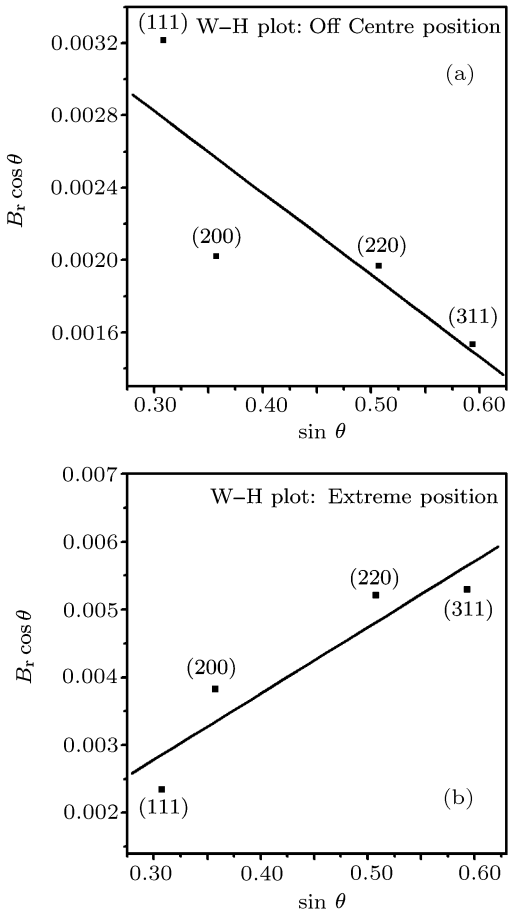


Fig. 4. Williamson–Hall plots for the samples carburized at 8 cm axial and (a) Off Centre and (b) Extreme positions.

a negative slope of W–H plot for the sample carburized at the Off Centre angular position (with comparatively high ion flux), which reveals the compressive nature of microstrains. However, the positive slope of the W–H plot for the sample treated at the Extreme angular position (with comparatively low ion flux) reveals a tensile nature of microstrains. These results are quite consistent with our previous investigations of DPF based surface processing of materials,[11] which show the conversion of stresses/strains from tensile to compressive by increasing the ion irradiance, and/or substrate temperature.

Figure 5 shows the variations of (a) average crystallite size and (b) microstrain versus axial distance, estimated from the W–H plots for the samples carburized at Off Centre and Extreme positions. The maximum average crystallite size is estimated to be $\sim$ 110 nm for the carburized surface at 12 cm axial and Off Centre angular position. It is revealed that the average crystallite size varies from $\sim$ 50 to 100 nm by moving the sample along the axial positions for all Off Centre positions. From the diffraction peaks recorded at Extreme angular positions, the average crystallite size is found to vary from $\sim$ 40 to 60 nm, which demonstrates the degradation in crystallinity of the film at larger angular positions, owing to lower energy flux of the ions which results in a lower substrate temperature. This also confirms the evolution of the lowest surface energy preferred (200) plane orientation at comparatively high substrate temperatures.

Systematic trends showing the presence of microstrains in the carburized layer at the three axial positions (8, 10 and 12 cm) for both the angular positions (Off Centre & Extreme) are depicted in Fig. 5(b) separately. For all Off Centre angular positions (i.e. for 8, 10 & 12 cm axial distances), small compressive strains show stress relieving by ion-assisted annealing of the samples bombarded with 20 shots, owing to the sufficient ion flux at these positions. Eventually, the average mirostrains are of low order in magnitude. At the 8 cm axial and Extreme angular position, tensile microstrains are pointing to deprived ion flux. However, the data of carburized samples at Extreme angular positions for 10 and 12 cm axial distances clearly show the conversion of microstrains from tensile to compressive. This is owing to the increase in ion flux at 10 and 12 cm axial and Extreme angular positions. In fact, at these positions, angular variation becomes low as compared with at 8 cm. Thus ion flux increases at higher axial distances (10 and 12 cm) having smaller angular variations compared with at lower distances (e.g. 8 cm) having larger angular variations according to the present geometry. This is due to significant reduction of ion flux with angular position.[12]

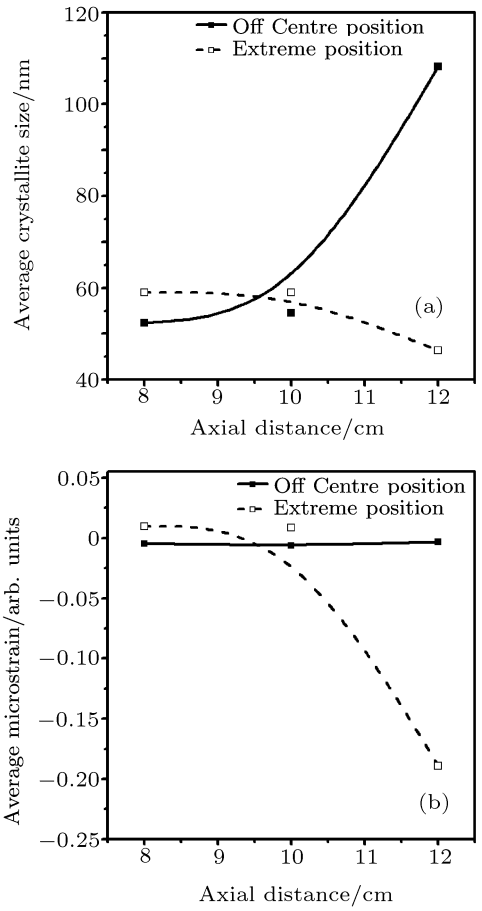


Fig. 5. Variations of (a) average crystallite size and (b) microstrain with axial distance, for the samples carburized at Off Centre and Extreme positions.

Raman spectroscopy of titanium carbide films has been reported rarely. A few Raman investigations have shown that Raman scattering in titanium carbide is due to the disorder induced by carbon vacancies.[35,36] Raman spectroscopy of the treated samples is performed by analysing phonon frequencies in a backscattering geometry with an Avantes AvaRaman micro-probe equipped with a continuous wave diode laser of 785 nm in wavelength.

Typical Raman spectra recorded for the samples treated at Off Centre and Extreme angular positions are presented in Fig. 6. The Raman spectra show two major doublets extending from $\sim$300 to 390 cm^{-1} and from $\sim$560 to 620 cm^{-1}, which respectively correspond to the acoustic and the optical modes of the phonon spectrum of titanium carbide.[35] The broadening of doublets is owing to the disorder in the carburized layer. The broad band extending from 690

to 830 cm^{-1} can be assigned to the second order scattering or some disorder-induced vibrational mode of TiC.[37] The amorphous nature of carbon is confirmed from D and G components (predominantly sp^2 bonded) appearing at around 1350 and 1556 cm^{-1} respectively. The Raman spectrum analysis confirms the carburizing of Ti in terms of a titanium carbide layer along with the adsorption of a-C. The Raman spectra clearly depict that at higher axial distances for an angular position (e.g. Off Centre), more prominent Raman peaks appear, owing to the increased ion flux at lower angular positions. These results are quite consistent with the previous results.[6]

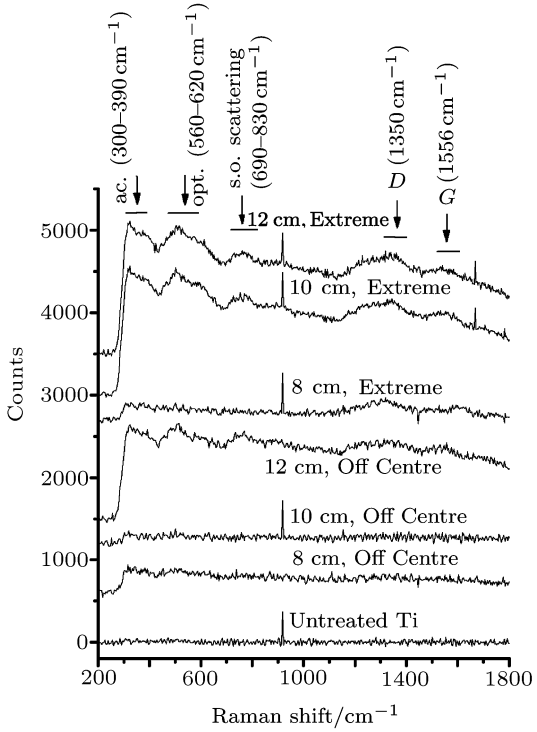


Fig. 6. Typical Raman spectra of the TiC thin films deposited at different axial and angular positions.

SEM micrographs exhibiting the surface morphologies of a virgin Ti sample and the sample exposed at the 8 cm axial and Extreme angular position are shown in Fig. 7. The virgin sample surface shows polishing marks that have almost been covered by carburizing. The micrograph of the carburized surface at the 8 cm axial and Extreme angular position shows an almost smooth layer with little grains seen uniformly over the surface. The DPF ion-assisted carburized layer exhibits granular microstructure. The DPF ion bombardment results in the restructuring of the substrate surface during collision cascades along with the interstitial implantation of carbon ions. The reaction of Ti sputtered or ablated with the gas phase carbon ions forms a TiC compound, which is deposited on the substrate as a layer. The evolution of a compound layer with distinct surface morphology on Ti substrate by the DPF ion based processing can be reviewed with details elsewhere.[7]

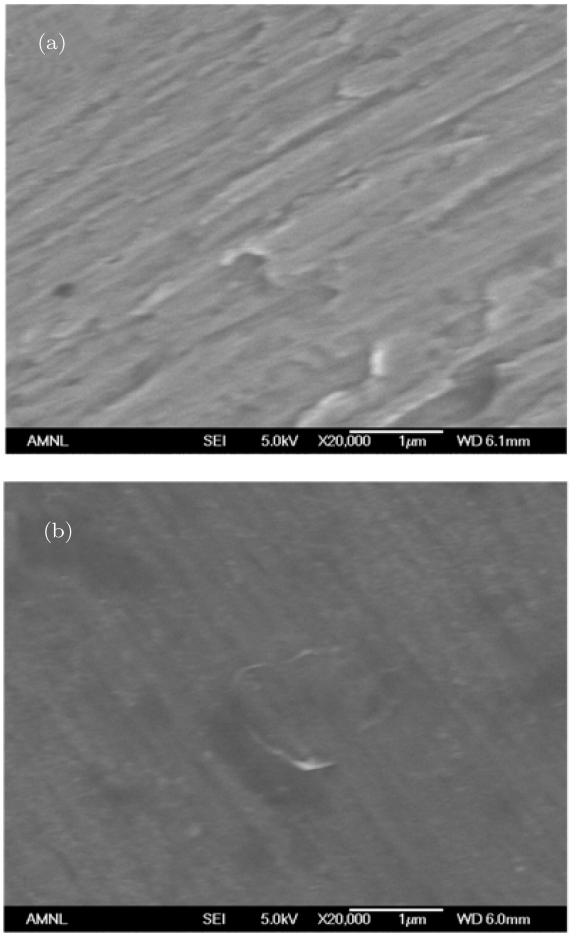


Fig. 7. Typical SEM micrographs of (a) untreated substrate surface and (b) TiC film surface deposited at the 8 cm axial and Extreme angular position.

Figure 8 shows EDS spectra of the unexposed and the carburized samples at the 8 cm axial and Off Centre angular position, along with its EDS maps (Ti Kα and C Kα). The EDS spectrum of the carburized sample (Fig. 8(b)) clearly displays a prominent carbon peak owing to the increased ion flux at this position. The spatial homogeneity of the carburized sample is exhibited by Ti Kα and C Kα EDS maps shown respectively in Figs. 8(c) and 8(d). The EDS data reveal that carbon content for the sample carburized at 8 cm reaches a maximum of up to 34.95 at.% at the Off Centre position and decreases significantly to 20.23 at.% at the Extreme position. Similarly, at 10 cm axial distance, carbon concentration varies from 41.54 at.%

at the Off Centre position to 32.21 at.% at the Extreme position. Table 1 provides EDS data for carbon composition of the carburized layer. The small fraction of Cu may be attributed to the sputtering of the electrode assembly. We observe that carbon content varies with sample position. The maximum carbon content is observed for typical positions ((10 cm, Off Centre) and (12 cm, Off Centre)) of the sample which respectively correspond to the minimum displacement with respect to the angular position. The remarkable decrease in carbon content at the 8 cm axial and Extreme position is owing to the abrupt fall of the DPF ion flux in comparison with the ion energy by varying angular position as investigated earlier.[4]

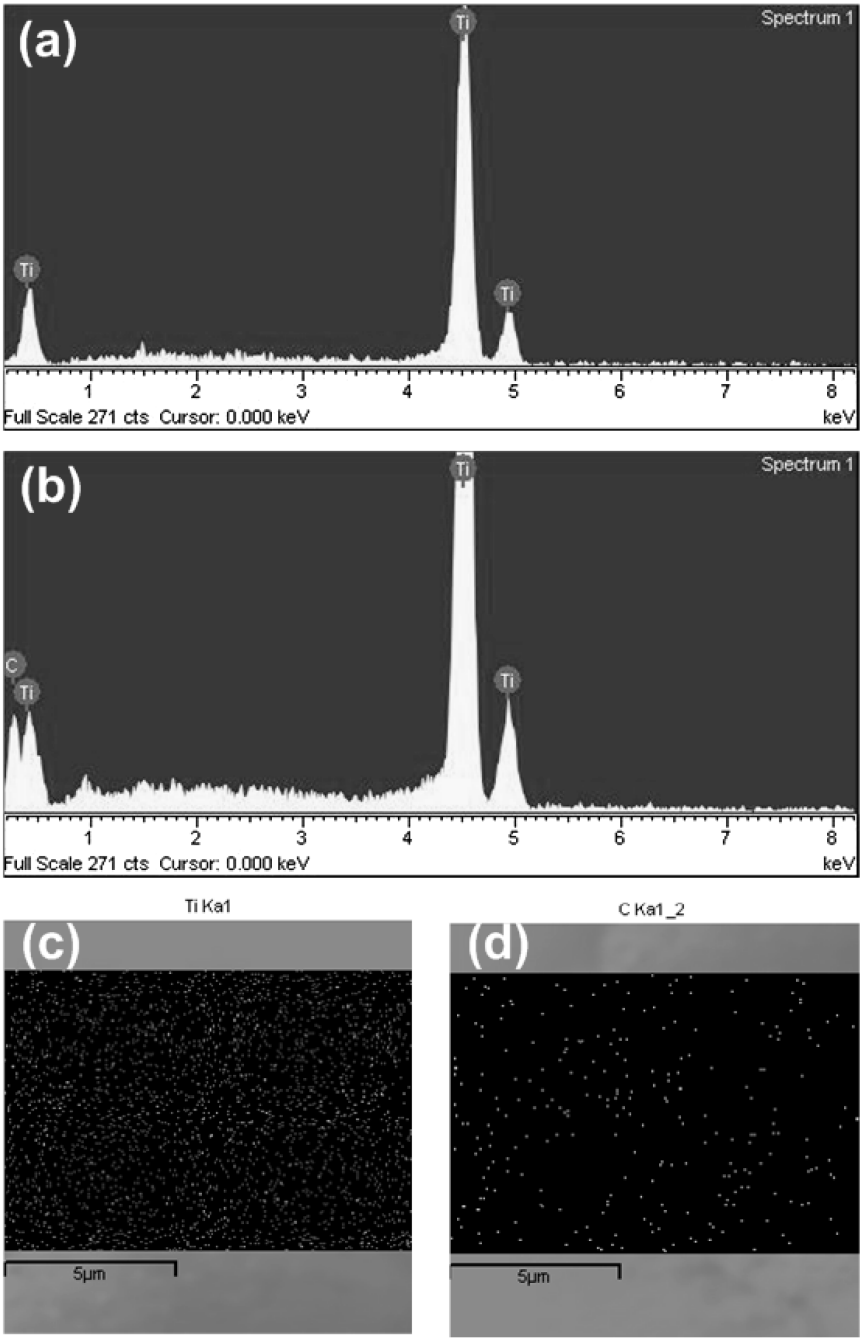


Fig. 8. Typical EDS spectra of (a) unexposed, (b) carburized samples at the 10 cm axial and Off Centre position, and corresponding EDS maps of (c) Ti Kα and (d) C Kα of the carburized sample.

Table 1. EDS data showing elemental concentrations (at.% & wt.%) estimated for the samples treated at different positions.

elemental concentrations	8 cm , Off Centre	10 cm, Off Centre	12 cm, Off Centre	8 cm, Extreme	10 cm, Extreme	12cm, Extreme
C (at. %)	34.95	41.54	41.82	20.23	32.21	37.32
C (wt. %)	11.87	15.05	14.89	5.98	10.65	12.99
Cu (at. %)	–	2.16	5.46	–	–	–
Cu (wt. %)	–	4.14	10.28	–	–	–

A Wilson Wolpert 401 MVA Vickers microhardness tester is used to measure the surface hardness of the carburized Ti substrate. Figure 9 shows the values of surface microhardness (HV) of the samples carburized at three different axial (8, 10 and 12 cm) and angular (Off Centre and Extreme) positions under several different imposed loads (10, 25, 50, 100, 200, 300, and 500 gf), each for a dwell time of 5 s. A significant improvement on surface hardness is observed for all the carburized samples in comparison with the case of the untreated sample. A maximum surface hardness of 264 MPa is measured for a typical sample carburized at the 8 cm axial and Extreme angular position. The improvement in mechanical strength may be attributed to the formation of TiC compound as well as the interstitial implantation of carbon ions. Moreover, stress-hardening owing to the momentum transfer by energetic ion impact is also contributing to the increase of surface hardening. The hardness value gradually decreases with load increasing and becomes comparable to that of untreated substrate. The abrupt fall in microhardness reveals a gradient of carbon concentration as well as ion-assisted stresses in the substrate-layer zone. These results confirm the improvement in mechanical behaviour of the carburized Ti surface in terms of surface hardness by employing a 1.5 kJ dense plasma focus device with methane discharge.

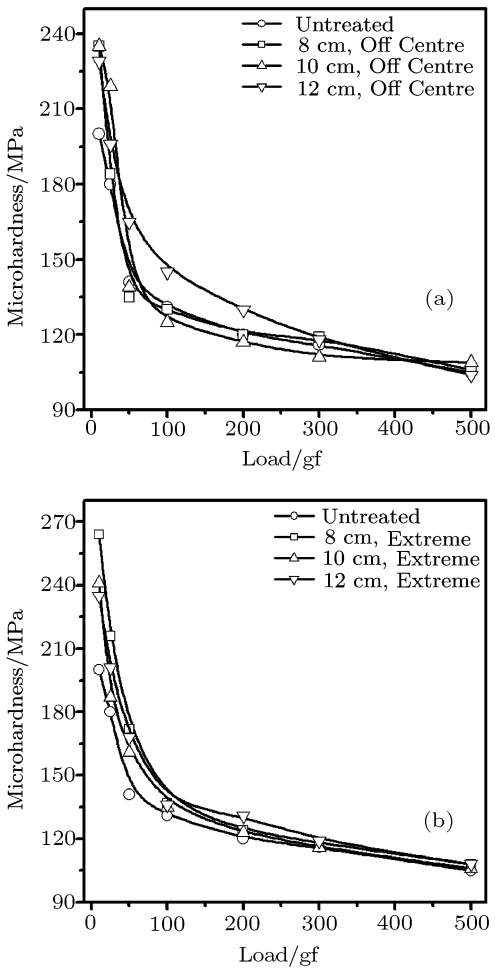


Fig. 9. Variation of microhardness (MPa) with indentation depth (μm) of the films deposited at different (a) axial and (b) angular positions. (1 gf=9.80665×10^{-3} N).

4. Conclusion

The room temperature carburizing of commercially pure Ti metal is accomplished by utilizing energetic carbon ions emitted from a 1.5 kJ plasma focus in CH_4 discharge. The texture analysis of carburized samples reveals that the preferred evolution TiC is dependent on sample position during the treatment. The texture coefficient is found to be a maximum of 1.19 when the sample is carburized at the 8 cm axial and Off Centre angular position. The average crystallite size evaluated from the TiC(200) preferred plane orientation is found to vary from $\sim$ 50 to 100 nm. Average microstrains developed in the carburized sample surfaces, owing to the bombardment of energetic ions, vary significantly from tensile to compressive for the samples placed at Off Centre positions, whereas almost the same levels of average microstrain are observed for those placed at Extreme positions.

The maximum average microstrain (compressive) calculated from the observed TiC plane orientation is 0.19, when the sample is carburized at the 8 cm axial and Extreme position. Raman spectroscopy of the samples confirms the carburizing of Ti by the presence of two major doublets appearing at ∼300–390 cm^{-1} and ∼560–620 cm^{-1} respectively, corresponding to the acoustic and the optical Raman active modes of titanium carbide, which is confirmed from D and G peaks appearing respectively at 1350 and 1556 cm^{-1} in the Raman spectra. The surface morphologies of films reveal the surface smoothening of Ti substrate with carbon content distributed uniformly in the carburized layer. The quantitative EDS analysis indicates that the carbon content in the layer is dependent mainly on ion flux and thus depletes swiftly by increasing the angular position rather than the axial position. The surface microhardness of the Ti sample is substantially improved after DPF based carburizing in CH_4 discharge.

References

[1] Ahmad S, Hussain S S, Sadiq M, Shafiq M, Waheed A and Zakaullah M 2006 *Plasma Phys. Control Fusion* **48** 745

[2] Ahmad S, Sadiq M, Shafiq M, Waheed A, Lee P and Zakaullah M 2006 *Plasma Sources Sci. Technol.* **15** 314

[3] Takao K, Honda T, Kitamura I and Masugata K 2003 *Plasma Sources Sci. Technol.* **12** 407

[4] Hassan M, Qayyum A, Ahmad R, Murtaza G and Zakaullah M 2007 *J. Phys.* D: *Appl. Phys.* **40** 769

[5] Lue J T, Yeh C K and Kuo Y Y 1983 *IEEE Electron Device Lett.* **4** 457

[6] Hassan M, Rawat R S, Lee P, Hassan SM, Qayyum A, Ahmad R, Murtaza G and Zakaullah M 2008 *Appl. Phys.* A **90** 669

[7] Rawat R S, Aggarwal V, Hassan M, Lee P, Springham S V, Tan T L and Lee S 2008 *Appl. Surf. Sci.* **255** 2932

[8] Rawat R S, Srivastava M P, Tandon S and Mansingh A 1993 *Phys. Rev.* B **47** 4858

[9] Gupta R and Srivastava M P 2004 *Plasma Sources Sci. Technol.* **13** 371

[10] Khan I A, Hassan M, Ahmad R, Qayyum A, Murtaza G, Zakaullah M and Rawat R S 2008 *Thin Solid Films* **516** 8255

[11] Hassan M, Ahmad R, Qayyum A, Murtaza G, Waheed A and Zakaullah M 2006 *Vacuum* **81** 291

[12] Sadowski M J, Gribkov V A, Kubes P, Malinowski K, Skladnik-Sadowska E, Scholz M, Tsarenko A and Zebrowski J 2006 *Phys. Scr.* T **123** 66

[13] Liu Z G, Guo J T, Ye L L, Li G S and Hu Z Q 1994 *Appl. Phys. Lett.* **65** 2666

[14] Brauer G, Anwand W, Nicht E M, Coleman P G, Knights A P, Schut H, Kogel G and Wagner N 1995 *J. Phys. Cond. Matt.* **7** 9091

[15] Sheats J R 1997 *Science* **277** 191

[16] Maiya P S, Erck R A and Moon B M 1998 *Surf. Coat. Technol.* **102** 218

[17] Besmann T M, Sinton D P, Lowden R A and Lee W Y In: Weimer A W (ed), 1997 *Carbide, Nitride and Boride Materials Synthesis and Processing* (London: Chapman & Hall) Ch. 22

[18] Randhawa H 1987 *Thin Solid Films* **153** 209

[19] Sundgren J E, Johansson B O, Karlsson S E and Hentzell H T G 1983 *Thin Solid Films* **105** 367

[20] Lowndes D H, Geohegan D B, Puretzky A A, Norton D P and Rouleau C M 1996 *Science* **273** 898

[21] Rawat R S, Lee P, White T, Ying L and Lee S 2001 *Surf. Coat. Technol.* **138** 159

[22] Comisar G G 1969 *Phys. Fluids* **12** 1000

[23] Greene J E, Sundgren J E, Hultman L, Petrov I and Bergstrom D B 1995 *Appl. Phys. Lett.* **67** 2928

[24] Junhua X, Geyang L and Mingyuan G 2000 *Thin Solid Films* **270** 45

[25] Hultman L, Sundgren J E, Greene J E, Bergstrom D B and Petrov I 1995 *J. Appl. Phys.* **78** 5395

[26] Ma C H, Huang J H and Chen H 2000 *Surf. Coat. Technol.* **133–134** 289

[27] Pelleg J, Zevin L Z, Lungo S and Croitoru N 1991 *Thin Solid Films* **197** 117

[28] Wolfe D E and Singh J 1998 *J. Mat. Sci.* **33** 3677

[29] Wolfe D E and Singh J 2000 *Surf. Coat. Technol.* **124** 142

[30] Akyuz I, Kose S, Atay F and Bilgin V 2006 *Semicond. Sci. Technol.* **21** 1620

[31] Barrett C S and Massalski T B 1966 *Structure of Metals* (New York: McGraw-Hill)

[32] Suryanarayana C and Norton M G 1998 *X-ray Diffraction: A Practical Approach* (Plenum Press) p125

[33] Williamson G K and Hall W H 1953 *Acta Metall.* **1** 22

[34] Kuzel Jr R and Klimanek P 1989 *J. Appl. Crystall.* **22** 299

[35] Klein M V, Holy J A and Williams W S 1978 *Phys. Rev.* B **17** 1546

[36] Amber M, Barsoum M W, El-Raghy T, Weiss I, Éclair S L and Liptak D 1998 *J. Appl. Phys.* **4** 5817

[37] Wipf H, Klein M V and Williams W S 1981 *Phys. Stat. Solidi* B **108** 489